Effect of Polydispersity on Diffusion in Random Obstacle Matrices

Hyun Woo Cho, Gyemin Kwon, Bong June Sung, and Arun Yethiraj

Phys. Rev. Lett. **109**, 155901 — Published 12 October 2012

DOI: 10.1103/PhysRevLett.109.155901

The effect of polydispersity on diffusion in random obstacle matrices

Hyun Woo Cho, Gyemin Kwon and Bong June Sung

Department of Chemistry, Sogang University, Seoul 121-742, Republic of Korea

Arun Yethiraj

Theoretical Chemistry Institute and Department of Chemistry,

University of Wisconsin, Madison, Wisconsin 53706

Abstract

The dynamics of tracers in disordered matrices is of interest in a number of diverse areas of physics such as the biophysics of crowding in cells and cell membranes, and the diffusion of fluids in porous media. To a good approximation the matrices can be modeled as a collection of spatially frozen particles. In this work we consider the effect of polydispersity (in size) of the matrix particles on the dynamics of tracers. We study a two dimensional system of hard disks diffusing in a sea of hard disk obstacles, for different values of the polydispersity of the matrix. We find that for a given average size and area fraction, the diffusion of tracers is very sensitive to the polydispersity. We calculate the pore percolation threshold using Apollonius diagrams. The diffusion constant, D, follows a scaling relation $D \sim (\phi_c - \phi_m)^{\mu-\beta}$ for all values of the polydispersity, where ϕ_m is the area fraction and ϕ_c is the value of ϕ_m at the percolation threshold.

PACS numbers:

The dynamics of tracers in disordered materials is of fundamental importance, and finds applications in a number of areas such as crowding effects in biophysics, the dynamics of fluids in porous media, and the diffusion of tracers in glasses. In most of these applications the matrix is structurally heterogeneous. Cell membranes, for example, contain many different types of large integral membrane proteins[1] of different sizes that act as obstacles to diffusing proteins and lipid molecules. There have been extensive studies on the diffusion of tracers in a sea of fixed obstacles but most have considered obstacles of uniform size[2–6]. In this Letter we consider the important case of polydisperse obstacles.

Polydispersity is ubiquitous in chemical and biological systems and is thought to play an important role in colloid physics,[7–9] granular materials,[10,11] and in cytoplasm mimics[12,13]. Although the presence of polydispersity is acknowledged, its impact on the tracer dynamics has not been systematically explored. In this work, we illustrate that the polydispersity can change the protein dynamics in a qualitative way even for the same area fraction and the same average size of macromolecules. We also show using percolation theory and the spatial tessellation that such seemingly different protein dynamics follows the same scaling relation.

The diffusion of proteins in cell membranes is significantly slower, by orders of magnitude, than in homogeneous lipid bilayers. The mean-square displacement, $W(t)$, of proteins often shows anomalous sub-diffusive behavior, i.e., $W(t) \sim t^{\alpha}$ with time exponent $\alpha < 1$. Experiments[2,5] using single particle tracking (SPT), fluorescence photobleaching recovery (FPR), and fluorescence correlation spectroscopy (FCS) techniques revealed that values of α ranged from 0.1 to 0.9 depending on the type of cells.

A qualitative understanding of the observed behavior is available. In cell membranes, cholesterol rich lipid domains and temporarily static proteins bound to cytoskeletons can become obstacles to protein diffusion. When the area fraction (ϕ_m) of such obstacles increases beyond a critical value, called pore percolation threshold area fraction (ϕ_c), percolating free area disappears and the proteins are confined in local pore space. For $\phi_m < \phi_c$, at short times the proteins do random walks in a fractal space and show anomalous sub-diffusion but recover the normal diffusive behavior at long times. At the percolation threshold ($\phi_m = \phi_c$), proteins show sub-diffusion at all length- and time-scales.

The dynamics of proteins near the percolation threshold can be described by scaling relations.[14–23] Diffusion coefficients D of tracers in a percolating free area scale as $D \sim (\phi_c - \phi_m)^{\mu-\beta}$ where μ and β are scaling exponents. The mean-square displacement $W(t)$ also

follows a scaling relation, i.e., $W(t) \sim t^{2/d_w} g((\phi_c - \phi_m) t^{1/(2\nu+\mu-\beta)})$ where $d_w = 2 + (\mu - \beta)/\nu$ and ν is the universal scaling exponent for the correlation length ξ ($\xi \sim |\phi_c - \phi_m|^{-\nu}$). $g(x)$ is a scaling function given by $g(x) = x^{\mu-\beta}$ for $x \to \infty$, $g(x) =$ constant for $x \to 0$, and $g(x) = (-x)^{-2\nu}$ for $x \to -\infty$. Determining the value of ϕ_c and the exponents is not trivial, especially for polydisperse systems, and is the subject of this work.

We study the dynamics of hard discs of diameter σ (which is our unit of length) in a two-dimensional space containing size polydisperse hard disc obstacles. The average diameter of obstacles, σ_m, is fixed at $\sigma_m = \sigma$. The simulation cell is a square of side length L with periodic boundary conditions in all directions. The number of obstacles (N_m) ranges from 12606 to 27303 and L ranges from 50 to 300. The obstacle area fraction (ϕ_m) ranges from 0.12 to 0.31. The polydispersity index is defined as $\frac{\sum d^2 \ P_d}{\{\sum d \ P_d\}^2}$, where d is the diameter of the obstacle and P_d is the probability of finding an obstacle with diameter d.

Initial configurations of the matrix are created by inserting obstacle discs at random locations so that they do not overlap with existing discs. The size of each inserted obstacle disc is sampled from a Gaussian distribution with mean σ and standard deviation $\delta_m = 0$, 0.5, and 1. Obstacles with diameter less than 0.1 are excluded from the configuration and the diameters of all discs are re-scaled so that the average diameter is σ. For $\delta_m = 0.5$ and 1, the polydispersity indices of rescaled discs are 1.66 and 2.15, respectively.

A small number (up to 573) of fluid particles are then inserted so that the fluid area fraction is 0.005. The fluid-fluid interactions are not significant but having more than one fluid particle results in better statistics. The fluid particles are inserted in a percolating region of the matrix so that there is no overlap with the matrix or other fluid particles. (We obtain percolating regions using the Apollonius diagrams discussed shortly.) If no percolating region is present the fluid particles are inserted at random locations.

Tracer dynamics is obtained using discontinuous molecular dynamics (DMD) simulations. DMD simulations employ an event-driven algorithm and evolve the system via successive collisions.[24] Hydrodynamic interactions are ignored in DMD and the dynamics is ballistic between collisions. Recent simulations[25] have shown, however, that the long time behavior is not affected by the short time dynamics. We use DMD because it is more efficient than Brownian dynamics or Monte Carlo simulations. For the diffusion of tracers in 3D random media identical results are obtained for the scaling exponents using either DMD or Monte Carlo. The mean-square displacement, $W(t) (\equiv \langle |\vec{r}_i(t) - \vec{r}_i(t=0)|^2 \rangle)$, is averaged over 5 to

10 configurations of the matrix, where $\vec{r}_i(t)$ is the position vector of the ith fluid particle at time t and $\langle \cdots \rangle$ denotes an ensemble average over both fluid and obstacle configurations.

There are three regimes in tracer dynamics as the obstacle area fraction is increased. For low values of ϕ_m the mean-square displacement, $W(t)$, is linear in time, t, i.e., the diffusion is normal. For very high values of ϕ_m the tracers are confined in non-percolating regions and $W(t) \sim t^0$ for long times. For intermediate times, $W(t) \sim t^\alpha$ over the time-scale of the simulation with $0 < \alpha < 1$, i.e., the tracers exhibit anomalous diffusion. These regimes are found for all the matrices studied, i.e., mono-disperse, and poly-disperse with δ_m=0.5 and 1.

For a given area fraction the tracers can exhibit qualitatively different dynamics in the different types of matrices. Figure 1 depicts $W(t)/4$ as a function of time for the three types of matrices, and for ϕ_m=0.24. For this matrix area fraction the tracers are confined in the mono-disperse matrix, show anomalous diffusion in the polydisperse matrix with δ_m=0.5, and normal diffusion in the polydisperse matrix with δ_m=1. The inset shows the apparent exponent α as a function of ϕ_m for the three matrices. The three regimes are apparent in this plot. The apparent exponent α drops continuously from 1 to its value at the percolation threshold as ϕ_m increases.

We determine the percolation threshold by mapping the system onto an effective *curvilinear* lattice. This is done by constructing an *Apollonius diagram*, where space is tessellated into many non-overlapping space-filling *curvilinear* polygons each of which contains one obstacle (see Figure 2). Any point in space belongs to a curvilinear polygon of an obstacle if and only if the obstacle is the closest one to the point, i.e., $|\vec{x} - \vec{r}_{mi}| - A_{mi} < |\vec{x} - \vec{r}_{mj}| - A_{mj}$, where $\vec{x}$ and $\vec{r}_{mi}$ are the position vectors of the point and the obstacle, respectively, $\vec{r}_{mj}$ is the position vector of any other obstacle and A_{mi} denotes the radius of the obstacle. The *vertex* in each polygon is defined as the point that is equidistant from the perimeter of the three neighboring obstacles, i.e., the center of the circle that is tangent to these obstacles. The circle is defined as a pore and its diameter is the pore diameter (σ_p). The curvilinear edge between two pores (vertices) is a hyperbola with two foci located at the centers of two obstacles that two pores share.(Figure 2(b))

The connectivity of the diagram is assigned by considering the possibility of solute passage.[4] When it is possible for a solute to go directly from one pore to a neighboring pore along an edge, the edge is considered to be connected, and disconnected otherwise.

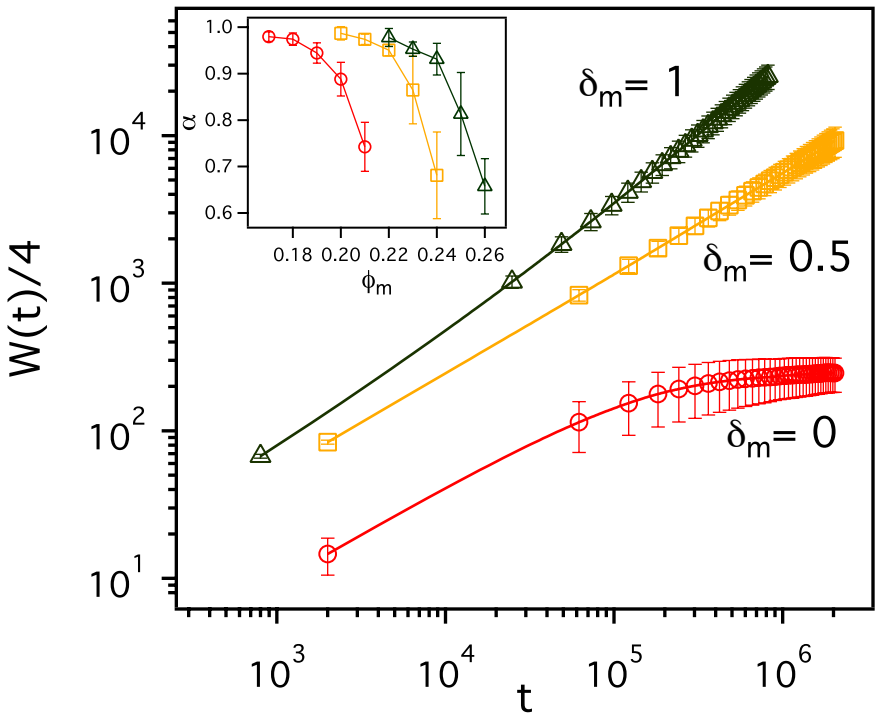

FIG. 1: The mean-square displacement, $W(t)$, as a function of time for δ_m=0 (monodisperse matrix), 0.5, and 1, for $\phi_m = 0.24$. The inset shows the apparent exponent α in $W(t) \sim t^{\alpha}$ as a function of ϕ_m.

The edge width, w, is defined as shortest distance between the perimeters of two obstacles, i.e., $w \equiv |\vec{r}_{m1} - \vec{r}_{m2}| - A_{m1} - A_{m2}$, where $\vec{r}_{m1}$ and $\vec{r}_{m2}$ are the positions of two of the obstacles that define a pore, and A_{m1} and A_{m2} are the corresponding radii. When w is smaller than the diameter (σ) of a solute (or tracer) the solute can not take the path and the edge is considered disconnected; otherwise it is determined to be connected. A cluster is defined as a set of vertices connected via at least one path and clusters of connected edges are searched for via a recursive algorithm. A percolating pore cluster, if any, is located by considering periodic boundary conditions. Under periodic boundary conditions, at least one vertex of a percolating network should be connected to its mirror image via a path across a simulation cell.

In order to obtain the pore percolation threshold area fraction ϕ_c, we estimate the probability (P) that a system contains a percolating pore network by calculating the ratio of the number of configurations with percolating networks to the number of all configurations generated. In a thermodynamic limit P undergoes a discontinuous transition

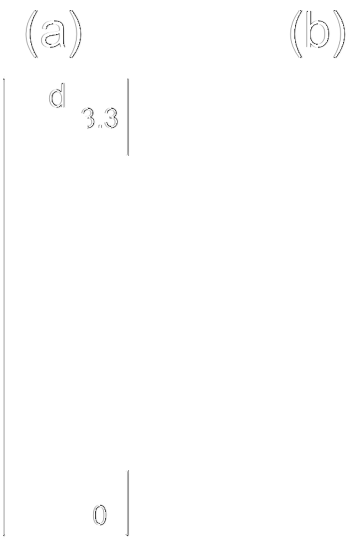

FIG. 2: (a) Apollonius diagram for a polydisperse medium with $\sigma_m = 1$, $\delta_m = 1$, and $\phi_m = 0.22$. Larger obstacles are represented by darker disks. Green lines and yellow lines are connected and disconnected edges, respectively. (b) Schematic of Apollonius tessellation. Shaded circles and open circles represent obstacles and pores, respectively.

at $\phi_m = \phi_c$. For a finite system, we fit values of P to a hyperbolic tangent function $P(\phi_m, L) = \frac{1}{2}(1 + tanh[(\phi_c(L) - \phi_m)/\Delta\phi])$, where $\phi_c(L)$ and $\Delta\phi$ are fitting parameters. The finite size effect on ϕ_c is well established with a scaling relation, i.e., $\phi_c(L) - \phi_c \sim L^{-1/\nu}$. Our values of $\phi_c(L)$ scales well with $\nu = 4/3$ and the y-intercept of the graph $\phi_c(L)$ vs. $L^{-1/\nu}$ is identified with ϕ_c.

The percolation threshold area fraction increases with increasing polydispersity. In general one would expect the percolation threshold to be higher with larger obstacles. However even if ϕ_m and the average obstacle diameter are fixed, the free area available to solutes increases as the polydispersity increases. This is because obstacles pack more efficiently in polydisperse media than in monodisperse media, and the free area accessible to solutes therefore increases with increasing polydispersity. We find that the pore percolation threshold area fractions $\phi_c = 0.21$, 0.24, and 0.26 for δ_m=0, 0.5, and 1, respectively.

We investigate the scaling behaviors of diffusion coefficients (D) and the mean-square displacements (W(t)). As depicted in the inset of Figure 3, D scales well as $(\phi_c - \phi_m)^{\mu-\beta}$ with $\mu - \beta \approx 1.6$ independent of δ. $W(t)t^{-2/d_w}$ also collapse well with the same value of $\mu - \beta$

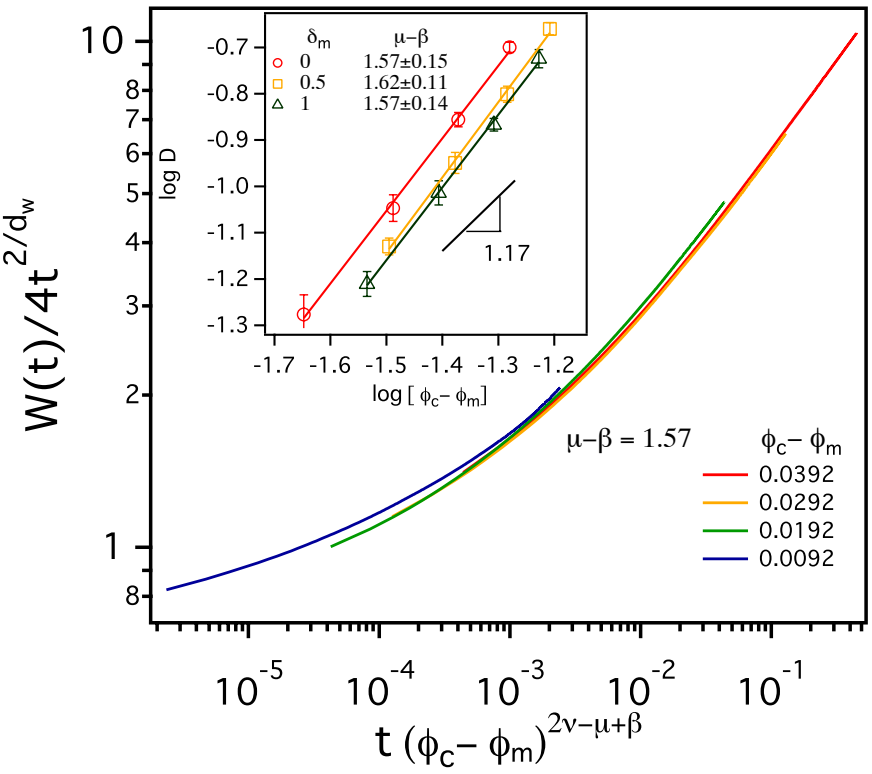

FIG. 3: The scaling function $W(t)t^{-2/d_w}$ as a function of $t(\phi_c - \phi_m)^{2\nu+\mu-\beta}$ for various values of ϕ_m for δ_m=1. In the inset is the log-log plot of diffusion coefficients as a function of $\phi_c - \phi_m$ for all values of δ_m.

onto a curve as a function of $t(\phi_c - \phi_m)^{2\nu+\mu-\beta}$. However, our simulation results for $\mu - \beta \approx 1.6$ deviate from the value (1.17) for lattice systems. Recent theoretical and simulation studies for a two-dimensional Lorentz model suggested that even though the non-universality of the transport exponent $\mu - \beta$ might originate from a sufficiently strong power-law singularity of the transition rate distribution between pores in three dimensions, narrow gaps responsible for the singularity would not be relevant in two dimensions and the transport exponent for lattices should be recovered.[18,19,21,23]

We cannot conclusively determine whether the exponent μ-β is universal, but our analysis suggests this is the case if the system is ergodic. In order to investigate whether the transport exponent $\mu - \beta$ is universal, we estimate the transition rate (W) between two pores and its distribution ($\rho(W)$).[17,22] If a tracer can collide many times with the three obstacles defining its pore before transitioning to a neighboring pore, and there is no correlation between the tracer entering and leaving the pore, one can invoke the ergodic hypothesis,

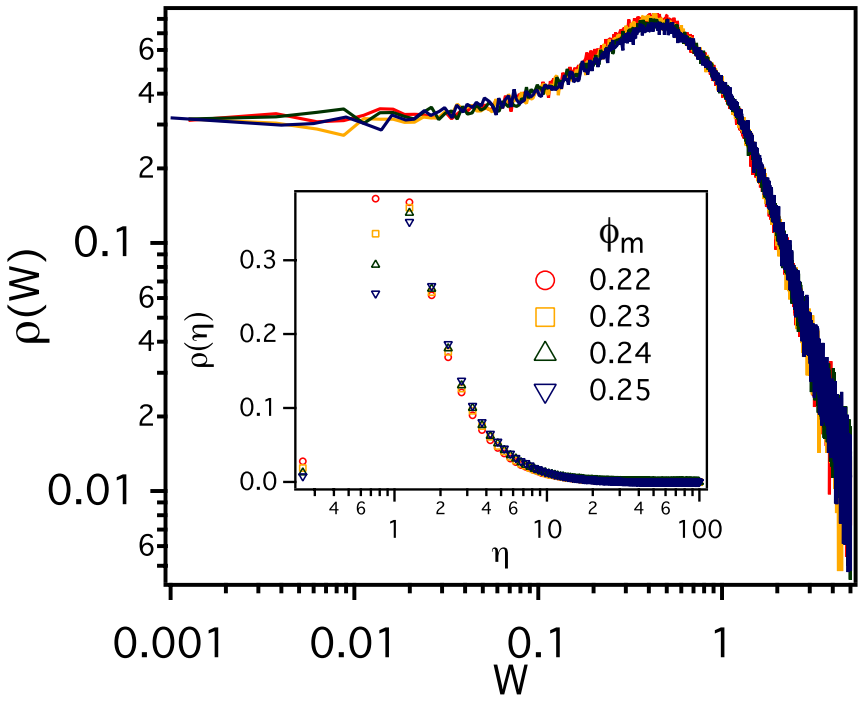

FIG. 4: The distributions of transition rate (W) for $\delta_m = 1$ and different values of ϕ_m. The inset shows the distributions of the expected number (η) of collisions per residence time of a tracer in a pore for $\delta_m = 1$.

and $W \sim (w-1)/A$, where A is the area of the region available for the center of the tracer in the pore and w is the edge width. As depicted in Figure 4, there is no singularity in $\rho(W)$'s for $\delta_m = 1$ for all values of ϕ_m, which implies that $\mu - \beta$ should be a universal exponent.

The ergodic hypothesis can be guaranteed only when the expected number ($\eta \equiv \pi/(w_1 + w_2 + w_3 - 3)$) of collisions per residence time of a tracer in a pore is large enough,[26] where $w_i (i = 1 \sim 3)$ is the edge width of a given pore. In case of a periodic Lorentz gas, η should be larger than 3.4. According to Machta and Zwanzig,[26] diffusion coefficients from molecular dynamics simulations were close to those from uncorrelated random walk models only for $\eta > 100$. As shown in the inset of Figure 4, the peak position of the distribution ($\rho(\eta)$) of η is far smaller than 3.4. The validity of the ergodic hypothesis is therefore questionable for small η and consequently we cannot conclusively determine if the exponent $\mu - \beta$ is universal.

In summary, we perform DMD simulations and spatial tessellation to investigate the effect of polydispersity in obstacle size on the solute diffusion. The solute diffusion can be

influenced significantly by the polydispersity because both the pore size distribution and the pore connectivity change significantly with the polydispersity, thus changing the pore percolation behavior of media. As the polydispersity index increases from 1 to 2.15, the pore percolation threshold area fraction increases by about 24%. Therefore, the solute diffusion may show all of normal, sub-diffusive, and confined dynamics behaviors depending solely on the polydispersity. This implies that the polydispersity in obstacle size should be an important element in the analysis of the experiments on the protein diffusion and structural heterogeneity in cell membranes. The spatial tessellation and DMD simulations employed in this study can be easily extended to study the dynamics and the structural heterogeneity in cell cytoplasms crowded with various macromolecules.

Acknowledgments

This material is based upon work supported by the National Science Foundation under Grant No. CHE-1111835 to A. Y. This work was also supported by the National Research Foundation of Korea (NRF) under Grant NRF-2011-220-C00030.

---

[1] D. M. Engleman, Nature **438**, 578 (2005).

[2] E. L. Elson, E. Fried, J. E. Dolbow, and G. M. Genin, Annu. Rev. Biophys. **39**, 207 (2010).

[3] N. Andrews, K. Lidke, J. Pfeiffer, A. Burns, B. Wilson, J. Oliver, and D. Lidke, Nature Cell Biology **10**, 955 (2008).

[4] B. Sung and A. Yethiraj, Phys. Rev. Lett. **96**, 228103 (2006).

[5] A. Kusumi, C. Nakada, K. Ritchie, K. Murase, K. Suzuki, H. Murakoshi, R. Kasai, J. Kondo, and T. Fujiwara, Annu. Rev. Bioph. Biom. **34**, 351 (2005).

[6] M. J. Saxton and K. Jacobson, Annu. Rev. Biophys. Biomol. Struct. **26**, 379 (1997).

[7] W. Schaertl and H. Sillescu, J. Stat. Phys. **77**, 1007 (1994).

[8] S. Auer and D. Frenkel, Nature **413**, 711 (2001).

[9] P. Sollich, Phys. Rev. Lett. **104**, 118302 (2010).

[10] S. Anishchik and N. Medvedev, Phys. Rev. Lett. **75**, 4314 (1995).

[11] X. Garcia, L. Akanji, M. Blunt, S. Matthai, and J. Latham, Phys. Rev. E **80**, 021304 (2009).

[12] D. Ridgway, G. Broderick, A. Lopez-Campistrous, M. Ru'aini, P. Winter, M. Hamilton, P. Boulanger, A. Kovalenko, and M. J. Ellison, Biophys. J. **94**, 3748 (2008).

[13] D. Bicout and M. Field, J. Phys. Chem. **100**, 2489 (1996).

[14] S. Havlin and D. Ben-Avraham, Adv. Phys. **51**, 187 (2002).

[15] C. P. James and G. T. Evans, J. Chem. Phys. **87**, 4056 (1987).

[16] T. Voigtmann and J. Horbach, Phys. Rev. Lett. **103**, 205901 (2009).

[17] B. Halperin, S. Feng, and P. Sen, Phys. Rev. Lett. **54**, 2391 (1985).

[18] J. Straley, J. Phys. C: Solid State Phys. **15**, 2343 (1982).

[19] T. Bauer, F. Hoefling, T. Munk, E. Frey, and T. Franosch, Eur. Phys. J. Special Topoics **189**, 103 (2010).

[20] S. vanderMarck, Phys. Rev. Lett. **77**, 1785 (1996).

[21] F. Hoefling and T. Franosch, Phys. Rev. Lett. **98**, 140601 (2007).

[22] J. Machta and S. Moore, Phys. Rev. A **32**, 3164 (1985).

[23] O. Stenull and H.-K. Janssen, Phys. Rev. E **64**, 056105 (2001).

[24] M. P. Allen and D. J. Tildesley, *Computer simulation of liquids* (Oxford University Press, New York, 1987).

[25] F. Höfling, T. Munk, E. Frey, and T. Franosch, J. Chem. Phys. **128**, 164517 (2008).

[26] J. Machta and R. Zwanzig, Phys. Rev. Lett. **50**, 1959 (1983).